

Density Functional Theory for the Photoionization Dynamics of Uracil

D. Toffoli

*The Lundbeck Foundation Center for Theoretical Chemistry
Department of Chemistry, University of Aarhus,
Langelandsgade 140, DK-8000 Aarhus C, Denmark and
CNR-INFM Democritos, National Simulation Center, Trieste, Italy*

P. Decleva

*Dipartimento di Scienze Chimiche, Università degli Studi di Trieste,
Via L. Giorgieri 1, I-34127 Trieste, Italy. and
CNR-INFM Democritos, National Simulation Center, Trieste, Italy*

F. A. Gianturco

*Dipartimento di Chimica, Università degli Studi "La Sapienza",
Piazzale A. Moro 5, I-00185 Roma, Italy.*

R. R. Lucchese

*Department of Chemistry, Texas A&M University,
College Station, Texas, 77843-3255, USA.*

(Dated: February 9, 2022)

Abstract

Photoionization dynamics of the RNA base Uracil is studied in the framework of Density Functional Theory (DFT). The photoionization calculations take advantage of a newly developed parallel version of a multicentric approach to the calculation of the electronic continuum spectrum which uses a set of B-spline radial basis functions and a Kohn-Sham density functional hamiltonian. Both valence and core ionizations are considered. Scattering resonances in selected single-particle ionization channels are classified by the symmetry of the resonant state and the peak energy position in the photoelectron kinetic energy scale; the present results highlight once more the site specificity of core ionization processes. We further suggest that the resonant structures previously characterized in low-energy electron collision experiments are partly shifted below threshold by the photoionization processes. A critical evaluation of the theoretical results providing a guide for future experimental work on similar biosystems.

INTRODUCTION

Research on electron- and photon-molecule collision dynamics is of both fundamental [1] and practical [2, 3] importance, for it is needed in a broad variety of applications, ranging from the manufacturing of semiconductor devices to atmospheric chemistry and physics. Theoretical studies are therefore needed not only for a fundamental understanding of the underlying dynamics, but also for the quantitative prediction of the appropriate data.

Following the pioneering work of Sanche and co-workers [4], electron interactions with biologically important molecules such as amino acids and nucleotides, have gained prominence, as it was convincingly suggested that resonant mechanisms induced by non-thermal low-energy electrons could be related to DNA and RNA lesions such as single strand breaks (SSBs) and double strand breaks (DSBs) [4].

Thus, the suggestion that metastable electron capture of the large amount of non-thermal secondary electrons produced upon the interaction of ionizing radiation with the cell environment [5] by the various DNA components could initiate the formation of SSBs and DSBs, stimulated a wealth of experimental work on electron collisions with gaseous [6–9] and thin films DNA and RNA bases [10]. Recently theoretical studies have also given a better understanding of these insights [11, 12].

Additionally, the notion of charge transfer and of electron flow along the π stack of nucleobases would benefit from the detailed knowledge of the response of the nucleotide moieties to excess negative charge [13]. Thus, the capability to stabilize an excess of charge in the nucleobases has been extensively investigated in recent years both experimentally and theoretically, (see for example refs. [13–22]) where electron attachment energies to several nucleobases including the title molecule were evaluated for the formation of both dipole- and valence-bound anions.

At variance with this promising and stimulating scenario, much less attention have been paid to the study of photoionization dynamics. In fact, even if the first measurement of the ionization potential (IP) of Uracil dates back to the late sixties [23] and since then UV and X-ray photoelectron spectra were measured and interpreted by a large number of investigators (see for example, [24–26], and references therein) none of these studies focused on the dynamical part of the photoionization process, namely, on the dependence of the intensity of the process on the incident photon energy (or, equivalently on the photoelectron kinetic

energy) and on the photoelectron ejection angle for a given final target state. The first five bands of the photoelectron spectra have been unambiguously assigned and associated with the three highest occupied π and the two (oxygen lone-pairs) nonbonding orbitals (n), the ordering being $\pi_1, n_1, \pi_2, n_2, \pi_3$ from the top of the photoelectron spectrum respectively [24], and the experimental ordering has been verified by theoretical semi-empirical and *ab-initio* CI calculations [24–26] and is being confirmed by the present work as well as we shall discuss below. High accurate gas phase ionization energies of Uracil, obtained by using electron-propagator methods have been published [27] and ionization energy thresholds in aqueous solutions have been discussed in even earlier work [28].

The close connection between shape-resonances in electron-molecule scattering and those in molecular photoionization has long been recognized [29]. In fact, although the long-range part of the scattering potential is drastically different in the two cases, the short-range part, is actually quite similar, being dominated by the interactions between the nuclei and the electrons common to both collision complexes. Therefore, since shape-resonant states are localized within the molecular volume, these should maintain their identity from one system to the other, although shifted in energy owing to the less effective screening in the scattering potential of the neutral molecule compared to that for the positive ion target. As a rule of thumb, therefore, photoionization shape resonances should have their counterparts in electron-molecule scattering experiments, albeit shifted by ~ 10 eV to higher electron energy [30].

The aim of the present study is to characterize, for the first time at the DFT level, both the outer valence and inner-shell photoionization dynamics of the Uracil molecule in a broad energy range, from threshold up to 100 eV of photoelectron kinetic energy. The method we use is essentially a one-electron method, thus we are unable to explicitly account for the variety of many-body effects inherently displayed in the complexity of electron- and photon-molecule collisions both at low and high energies [31], but it has consistently afforded a realistic description of one-electron resonant processes (for a review see ref. [32]). Further, its LCAO version [33] is applicable to fairly large molecular systems with a markedly lower computational cost when compared to earlier, realistic independent-electron *ab-initio* methods [30].

The paper is organized as follows: the next two sections describe our theoretical method and the computational details. In Section IV we will discuss our results for the core- and

outer-valence ionizations. Our conclusions and perspectives are then summarized in the final section.

COMPUTATIONAL METHOD

Dynamical quantities describing the photoionization process from Uracil are calculated in the framework of the DFT approach, by employing a Fortran90 suite of codes fully described in earlier publications [33, 36] so we only sketch here their salient features. The present formulation affords a one-electron picture of the scattering process, thereby casting the collisional problem as given via the use of an effective potential according to the Kohn-Sham scheme [37]. The escaping electron is deflected by such a potential containing the molecular ground state density, $\rho(\vec{r})$, and conventionally separated into direct (Hartree), V_H and exchange-correlation, V_{xc} terms:

$$h_{KS}\varphi_i = \epsilon_i\varphi_i \quad (1)$$

with

$$h_{KS} = -\frac{1}{2}\nabla^2 - \sum_{i=1}^N \frac{Z_i}{|\vec{r} - \vec{R}_i|} + \int \frac{\rho(\vec{r}')}{|\vec{r} - \vec{r}'|} d\vec{r}' + V_{xc}[\rho(\vec{r})] \quad (2)$$

The interaction potential is then expanded in a composite basis set, whose nature constitute the key-feature of the present LCAO approach [33]. The LCAO basis set consists in a large single center expansion (SCE) located at a chosen origin (usually the center of mass of the molecule)

$$\chi_{nlh}^{p\mu, SCE} = \frac{1}{r} B_n(r) \sum_m b_{lmh}^{p\mu} Y_{lm}^R(\theta, \phi) \equiv \frac{1}{r} B_n(r) X_{lh}^{p\mu}(\theta, \phi), \quad (3)$$

and supplemented by functions of the same type, located on the off-center arbitrary positions j

$$\chi_{nlh}^{p\mu, i} = \sum_{j \in Q_i} \frac{1}{r_j} B_n(r_j) \sum_m b_{lmh, j}^{p\mu} Y_{lm}^R(\theta_j, \phi_j), \quad (4)$$

In Equation (4), index i runs over the non-equivalent nuclei, j runs over the set of equivalent nuclei, Q_i , and gives the origin of the off-center spherical coordinates (r_j, θ_j, ϕ_j) . The sets of coefficients $b_{lmh}^{p\mu}$ and $b_{lmh, j}^{p\mu}$ define the unitary transformations between real spherical

harmonics $Y_{lm}^R(\theta, \phi)$ and the symmetry adapted angular basis sets [38] which transform as the μ th element of the p th irreducible representation (IR) of the molecular point group. B_n is the n th spline one-dimensional function [39]. The B -splines are built over the radial interval $[0, R_{max}^{SCE}]$ for the set $\chi_{nlh}^{p\mu, SCE}$, and over the intervals $[0, R_{max}^i]$ for the off-center functions $\chi_{nlh}^{p\mu, i}$. In the LCAO implementation the spheres of radius R_{max}^i are not allowed to intersect each other; furthermore, in order to assure continuity of the second derivatives over the surfaces of the spheres, for every $\chi_{nlh}^{p\mu, i}$ set, the last three splines are deleted.

With this basis set, Eq. (1) is recast into an algebraic eigenvalue problem, and bound state solutions (orbitals φ_i) are obtained with standard generalized diagonalization of the hamiltonian matrix, whereas scattering states are extracted as the set of linearly independent eigenvectors of the energy-dependent matrix $A^\dagger A$:

$$A^\dagger A(E)c = ac \quad (5)$$

corresponding to minimum modulus eigenvalues [33]. In Eq. (5) $A(E) = H - ES$, H and S being the hamiltonian and overlap matrices over the LCAO basis set respectively. Diagonalization is efficiently performed with the inverse iteration procedure [40]. Partial-wave independent solutions of Eq. (5) are then normalized to incoming wave boundary conditions [41] and partial cross sections and asymmetry parameters are evaluated with standard expressions [42].

COMPUTATIONAL DETAILS

The DFT calculations have been executed as follows. The ground state electron density of Uracil at the experimental equilibrium geometry [47] for its diketo form [48] and assuming a C_s symmetry, was calculated with the ADF package [49, 50] employing an all-electron double- ξ plus polarization (DZP) basis set of Slater-type orbitals, taken from the ADF database. Such a density is then used to build the h_{KS} hamiltonian (Cfr. Eq. (1)). The LB94 xc potential [51] has been used because of its correct asymptotic behavior [52].

The fixed-nuclei photoionization calculations used an SCE expansion up to $l_{max}^{SCE} = 15$ for expanding the bound molecular and continuum orbitals with the SCE placed on the centre of mass (C.M.) of the molecule. B -spline functions of order 10 are employed in the calculation, and defined over a linear radial grid with a step size of 0.2 a.u. extending up to

$R_{max}^{SCE} = 20$ a.u.. The intervals were supplemented with additional knots near the position of the nuclei in order to gain flexibility of the basis set in the region of the core orbitals. The maximum angular momenta l_{max}^i employed in the off-center expansions were $l_{max}^i = 1$ and $l_{max}^i = 2$ for the hydrogens and the heavier atoms respectively, whereas carefully selected values for R_{max}^i defining the off-center radial grids range from 0.75 a.u. (hydrogen sites) to 1.24 a.u. (oxygen sites).

Valence IP's of Uracil were also evaluated with the ADF program by using the Slater's transition-state approximation [53], a Slater-type basis set of triple- ξ plus polarization (TZP) quality and the Becke-Perdew [54, 55] *xc* potential.

RESULTS AND DISCUSSION

In this section we will present and discuss photoionization cross sections and asymmetry parameters profiles calculated with the LCAO DFT scattering code for selected orbital ionizations. Specifically the K 1s ionizations of Oxygen Nitrogen and Carbon atoms, and the outer-valence ionizations giving rise to the first five resolved bands of the photoelectron spectrum [24–26]. Although results have been obtained also for inner-valence orbital ionizations we will not attempt to discuss and rationalize them here, since single-electron approximation based theories are well-known to loose of their predictive power in the inner-valence region of the spectrum. (magari mettere su un documento EPAPS?) Figure 1 reports the chemical structure of Uracil and the numbering scheme adopted in the present work, while the experimental IPs [24–26] are reported in Table I, together with theoretical values taken from the literature [27], and results of DFT bound-state calculations using two different *xc* potentials and ground-state (core ionizations) or transition-state (valence ionizations) configurations. Focusing on the core IP's, fair agreement is found between experimental [56] and ground-state LB94 IP's, the latter being systematically overestimating the core IP's energies by as much as 5 eVs. Nonetheless, the LB94 ground-state calculations are able to account for the small differences among the various C 1s IP's, in other words the chemical shifts of carbon atoms are nicely reproduced, as usually found when applying DFT to core ionizations of large molecules (see e.g. [57]). The observed trend in the chemical shifts is readily rationalized by considering the bond connectivity of the carbon atoms, in particular with the more electronegative nitrogen and oxygen centers. These results once more un-

derline the peculiarity of core ionization studies to provide qualitative informations of both electronic and structural type, pertaining to the different sites probed by core ionization.

For the five outermost valence IP's there is a broad agreement between theoretical results and experimental data: use of the Becke-Perdew [54, 55] *xc* potential and the transition-state procedure with a TZP basis set has allowed to account fairly well of relaxation and correlation effects, giving results of comparable quality of those obtained with the P3 *Ab-Initio* procedure [27].

Photoelectron dynamics of core ionizations

The LCAO-DFT partial cross section and asymmetry parameter profiles for the core ionizations, Oxygen 1s ($1a'$ and $2a'$ ionizations), Nitrogen 1s ($3a'$ and $4a'$ ionizations) and Carbon 1s ($5a'$ through $8a'$ ionizations), are plotted in Figure 2 and Figure 3 respectively. The dynamical observables are plotted on the photoelectron kinetic energy scale because it will prove convenient for the purpose of identifying striking similarities in the scattering dynamics for the various final ionic states. One readily sees that the two Oxygen 1s ionization cross sections behave similarly, due to nearly identical initial states (upper left frame of Fig. 2). The same is true for the Nitrogen 1s ionizations (upper right frame of Figure 2). Three low-energy shape-resonances are clearly discernible in the O 1s ionization channels, a more intense one centered at about 7.5 eV of photoelectron kinetic energy, located in between two less intense features and superimposed on a strong background. A sharper prominent resonance characterize the low-energy scattering dynamics following the N 1s ionizations, with a peak energy of about 6.8 eV. The resonant peak shows up more clearly in the $N_3 1s^{-1}$ continua, rather than in the N_1 one, where the cross section is more structured toward threshold. In the lower frames of Fig. 2 we have reported the cross section profiles for the four C $1s^{-1}$ ionizations. These are conveniently plotted in two separate groups, according to the similarities or differences shared in their near-threshold behavior. Thus one can easily find marked analogies in the $5a'$ and $6a'$ partial cross sections over the whole electron kinetic energy range: both display a fairly strong resonant peak at about 7 eV and a weaker one at about 14.1 eV, after which the two profiles can be nearly superimposed on the scale of the Figure. The cross section profiles for the $7a'$ and $8a'$ orbital ionizations behave quite similarly, even if two separate features at 7.1 and 14.1 eV in the $7a'$ continua

eventually coalesce into a single broad peak in the $8a'$ continua, and the two cross section profiles behave markedly different when approaching threshold. It is worth noting that all core ionization cross sections show a broad hump at about 35 eV of photoelectron kinetic energy, a feature which should be connected with inefficient trapping of the photoelectron by high- l partial waves of the one-particle effective scattering potential. Asymmetry parameter profiles, plotted in Fig. 3, behave similarly: marked analogies are again found within the four groups of core ionizations. In every case the profiles are quite structured, a clear consequence of the wealth of resonant states that characterize the low-energy scattering dynamics of Uracil core ionization. The high-energy shape-resonant state, which is predicted to appear in all the ionization continua, causes stronger modulations on the angular distributions of the two O $1s^{-1}$ and C₂ and C₄ $1s^{-1}$ continua when compared with those leading to the remaining core-ionized target states. Furthermore, by inspecting the partial photoionization cross section profiles for the two dipole-allowed continuum symmetries (not reported in the figures) it is found that for every target ion the continuum resonant states belong to the a' symmetry (*vide infra*).

Photoelectron dynamics of outer valence ionizations

The LCAO-DFT partial cross section and asymmetry parameter profiles for the outermost photoelectron band orbital ionizations are plotted in Figures 4 for the π orbitals ($3a''$, $4a''$ and $5a''$) and in Figure 5 for the (oxygen lone pairs) nonbonding n orbitals ($23a'$ and $24a'$). As anticipated, the richness of resonant features characterizing the inner-shell ionizations is partially lost when moving to the outer-valence ionizations, even if strong and well defined features clearly show up in at least two continuum channels (corresponding to the $4a''$ and $23a'$ ionizations, central and upper panels of Fig. 4 and Fig. 5 respectively). Focusing our attention to the π ionizations (Figure 4) the cross section profiles share a common behavior: a steep rise toward threshold and a rapid monotonic decrease for higher excitation energies. However, only in the $4a''$ continua above-threshold shape resonances are found, where both the $\epsilon a'$ and $\epsilon a''$ channels are predicted to be resonant. Partial and total cross section profiles for the photoionization out of the $3a''$ orbital rise steeply at threshold, without any noticeable slope change, and a resonant state, albeit very close to threshold is visible in the $\epsilon a''$ continuum of the $5a''$ ionization and is barely apparent in the summed profile (lower

left panel of Figure 4). The corresponding asymmetry parameters, also plotted in Figure 4 are almost featureless, with the exception of that corresponding to the $4a''$ ionization which displays a near-threshold oscillation typical of the formation of a resonant state, as discussed above.

Partial and total cross sections for the remaining two valence ionizations considered ($23a'$ and $24a'$ orbitals) are predicted to be quite more structured and are plotted in Figure 5. Both cross sections show strong oscillations near threshold in the $\epsilon a'$ continuum, and a rather broad peak above 30 eV in the $\epsilon a''$ channel. Similarly, the asymmetry parameter profiles are rather structured, both at low and high photon energies. Table II lists, for every orbital ionization analyzed so far, the peak energy positions (on the photoelectron kinetic energy scale) and the symmetries of the resonant states identified.

Correlation with electron-molecule scattering experiments

As readily apparent from Table II, computed photoionization dynamics of Uracil reveals a wealth of near-threshold structures, especially in core ionizations. For core ionizations several resonant states show up at roughly the same energy positions into several final target state channels. This is the case, for example, for the resonant $\epsilon a'$ states with peak energy positions at about 7 eV, 14.1 eV and about 34 eV of photoelectron kinetic energy. As an attempt to correlate computed photoionization resonant states with those found in electron-molecule scattering calculations [11, 12] we then decided to analyze the resonant wave functions by inspecting the *dipole-prepared* continuum wave function [34]. Therefore the continuum wavefunction corresponding to the symmetry and peak energy positions listed in Table II have been transformed accordingly [34] and analyzed. Nearly all the *pseudo*-bound states are diffuse in nature, extending thorough the whole molecular skeleton. Also no hint of resonant states that could be correlated with the metastable anionic state experimentally found at about 9 eV in electron-scattering experiments were found. This is quite expected in view of the different nature of the interaction potential in photoionization compared to electron-neutral target collision processes. We are therefore led to the conclusion that all relevant resonant states characterized in low-energy electron collision processes [11, 12], shift below threshold in photoionization. For the purpose of comparison with the present study it would be interesting to investigate higher energy electron-collision processes; modeling these high

energy interactions proves however a more difficult theoretical task since electronic excitation channels need to be considered as well.

Finally, one last comment about our theoretical results should be made. Since vibrational couplings are completely neglected in our treatment of the photoionization dynamics and those invariably shorten the life-time of metastable resonant states, a broadening of the resonant structures will result with the consequence that the beautiful structuring of core ionizations cross sections predicted in the framework of the fixed-nuclei approximation will be partially lost.

CONCLUSION

The paper presents a theoretical investigation of the photoionization process from the biologically important RNA base Uracil. To the author's knowledge this is the first theoretical investigation of photoionization dynamics from the Uracil molecule to date. The theoretical method employed adopts a density functional theory description of photoionization dynamics and takes advantage of a multicentric basis set of B -spline functions for obtaining results that are converged within the one-electron effective DFT hamiltonian. Several peculiar results were found that demand for an experimental investigation and verification, especially in core ionizations. We predict inner-shell photoionization dynamics to be characterized by the presence of several resonant states and theoretical results can be rationalized as a consequence of the inherent site specificity of core ionization processes. Computed resonant states have been classified based on the symmetry of the resonant state and the peak energy position of the spectral features. Correlation with computed resonant structures found in low-energy electron-molecule collision experiments has been attempted: we suggest that transient negative ion states characterized in low-energy scattering experiments are not visible in photoionization but shifted in the discrete region of the spectrum. It is believed that the present theoretical results could be valuable in guiding and assisting future experimental work on this biologically important molecule.

ACKNOWLEDGMENTS

One of us (D. T.) would like to acknowledge CNR-INFM Democritos for a post-doctoral research fellowship.

-
- [1] *Electron Collisions with Molecules, Clusters, and Surfaces*, edited by H. Ehrhardt and L. A. Morgan (Plenum, New York, 1994).
 - [2] A. Grill, *Cold Plasma in Material Fabrication* (IEEE, New York, 1994).
 - [3] *Atmospheric Physics and Chemistry*, edited by H. S. W. Massey and D. R. Bates (Academic, New York, 1982).
 - [4] B. Boddaiffa, P. Cloutier, D. Hunting, M. A. Huels, and L. Sanche, *Science*, **287**, 1658 (2000).
 - [5] 1. International Commission on Radiation Units and Measurements, *ICRU report 31* (ICRU, Washington, DC, 1979)
 - [6] G. Hanel, B. Gstir, S. Denifl, P. Scheier, M. Probst, B. Farizon, M. Farizon, E. Illenberger, and T. D. Mark, *Phys. Rev. Lett.* **90**, 188104 (2003).
 - [7] H. Abdoul-Carime, M. A. Huels, F. Brünig, E. Illenberger, and L. Sanche, *J. Chem. Phys.* **113**, 2517 (2000).
 - [8] S. Denifl, S. Ptasińska, G. Hanel, B. Gstir, M. Probst, P. Scheier, and T. D. Märk *J. Chem. Phys.* **120**, 6557 (2004).
 - [9] S. Feil, K. Gluch, S. Matt-Leubner, P. Scheier, J. Limtrakul, M. Probst, H. Deutsch, K. Becker, A. Stamatovic, and T. D. Märk *J. Phys. B.* **37**, 3013 (2004).
 - [10] M.-A. Hervé du Penhoat, M. A. Huels, P. Cloutier, J.-P. Jay-Gerin, L. Sanche, *J. Chem. Phys.* **114**, 5755 (2001).
 - [11] A. Grandi, F. A. Gianturco, and N. Sanna, *Phys. Rev. Lett.* **93**, 048103 (2004).
 - [12] F. A. Gianturco, and R. R. Lucchese, *J. Chem. Phys.* **120**, 7446 (2004).
 - [13] J. Schiedt, R. Weinkauff, D. M. Neumark, and E. W. Schlag, *Chem. Phys.* **239**, 511 (1998).
 - [14] C. Desfrancois, H. Abdoul-Carime, J. P. Schermann, *J. Chem. Phys.*, **104**, 7792 (1996).
 - [15] C. Desfrancois, V. Periquet, Y. Bouteiller, and J. P. Schermann, *J. Phys. Chem. A* **102**, 1274 (1998).
 - [16] J. H. Hendricks, S. A. Lyapustina, H. L. de Clercq, J. T. Snodgrass, K. H. Bowen, *J. Chem.*

- Phys., **104**, 7788 (1996).
- [17] J. H. Hendricks, S. A. Lyapustina, H. L. de Clercq, K. H. Bowen, J. Chem. Phys., **108**, 8 (1998).
 - [18] J. Smets, D. M. A. Smith, Y. Elkadi, L. Adamowicz, J. Phys. Chem. A, **101**, 9152 (1997).
 - [19] J. Smets, W. J. McCarthy, L. Adamowicz, J. Phys. Chem., **100**, 14655 (1996).
 - [20] K. Aflatooni, G. A. Gallup, and P. D. Burrow, J. Phys. Chem. A, **102**, 6205 (1998).
 - [21] S. S. Wesolowski, M. L. Leininger, P. N. Pentchev, and H. F. Schaefer III, J. Am. Chem. Soc. **123**, 4023 (2001).
 - [22] O. Dolgounitcheva, V. G. Zakrzewski, and J. V. Ortiz, Chem. Phys. Lett. **307**, 220 (1999).
 - [23] C. Lifshitz, E. D. Bergmann, B. Pullman, Tetrahedron Lett., (1967), 4583.
 - [24] T. J. O'Donnell, P. R. LeBreton, J. D. Petke, and L. L. Shipman, J. Phys. Chem., **84**, 1975 (1980).
 - [25] S. Urano, X. Yang, and P. R. LeBreton, J. Mol. Struct. **214**, 315 (1989).
 - [26] M. Kubota, and T. Kobayashi, J. Electron. Spectr. Relat. Phenom. **82**, 61 (1996).
 - [27] O. Dolgounitcheva, V. G. Zakrzewski, and J. V. Ortiz, Int. J. Quantum Chem. **80**, 831 (2000).
 - [28] C. E. Crespo-Hernández, R. Arce, Y. Yasuyuki Ishikawa, L. Gorb, J. Leszczynski, and D. M. Close, J. Phys. Chem., **108**, 6373 (2004).
 - [29] J. L. Dehmer, D. Dill, in: *Symp. on Electron-Molecule Collisions*, edited by I. Shimamura and M. Matsuzawa (Univ. of Tokio Press, Tokio, 1979) p. 95.
 - [30] J. L. Dehmer, A. C. Parr, S. H. Southworth in: *Handbook on Synchrotron Radiation*, Vol. 2, edited by G. W. Marr (Elsevier Science Publishers B.V. 1987) p. 241.
 - [31] R. W. Zurales, R. E. Stratmann, S. Botting, R. R. Lucchese, in: *Photon and Electron Collisions with Atoms and Molecules*, edited by P. G. Burke and C. J. Joachain (Plenum, New York, 1997), p. 109.
 - [32] H. Bachau, E. Cormier, P. Decleva, J. E. Hansen, and F. Martin, Rep. Prog. Phys., **64**, 1601 (2001).
 - [33] D. Toffoli, M. Stener, G. Fronzoni, and P. Decleva, Chem. Phys., **276**, 25 (2002).
 - [34] M. Stener, G. Fronzoni, D. Toffoli, P. Colavita, S. Furlan, and P. Decleva, J. Phys. B: At. Mol. Opt. Phys., **35**, 1421 (2002).
 - [35] R. R. Lucchese, F. A. Gianturco, Int. Rev. Phys. Chem., **15**, 429 (1996).
 - [36] M. Stener, G. Fronzoni, D. Di Tommaso, and P. Decleva, J. Chem. Phys., **120**, 3284 (2004).

- [37] R. G. Parr, and W. Yang, *Density Functional Theory of Atoms and Molecules* (Oxford University Press, New York, 1989).
- [38] S. L. Altmann, and P. Herzig, *Point-Group Theory Tables*(Oxford University Press, Oxford, 1994).
- [39] C. de Boor, *A Practical Guide to Splines* (Springer, New York, 1978).
- [40] M. Brosolo, and P. Decleva, Chem. Phys., **159**, 185 (1992).
- [41] J. R. Taylor, *Scattering Theory*,(Wiley, New York, 1978).
- [42] N. Chandra, J. Phys.B: Atom. Mol. Opt. Phys., **20**, 3405 (1987).
- [43] S. J. Hara, J. Phys. Soc. J. Jpn, **22**(1967), 710.
- [44] A.P.P. Natalense, and R. R. Lucchese, J. Chem. Phys. **111**, 5344 (1999).
- [45] D. Toffoli, M. J. Simpson, R. R. Lucchese, Phys. Rev. A **69**, 062712 (2004).
- [46] R. E. Stratmann, R. R. Lucchese, J. Chem. Phys., **97**, 6384 (1992).
- [47] R. F. Stewart, L. H. Jensen, Acta Crystallogr., **23**, 1102 (1967).
- [48] J. Rejnek, M. Hanus, M. Kabeláč, F. Ryj’áček, and P. Hobza, Phys. Chem. Chem. Phys., **7**, 2006 (2005).
- [49] E. J. Baerends, D. E. Ellis, and P. Ros, Chem. Phys., **2**, 41 (1973).
- [50] C. Fonseca-Guerra, J. G. Snijders, G. te Velde, and E. J. Baerends, Theor. Chem. Acc., **99**, 391 (1998).
- [51] R. Van Leeuwen, E. J. Baerends, Phys. Rev. A, **49**, 2412 (1994).
- [52] , G. D. Mahan, K. R. Subbaswamy *Local Density Theory of Polarizability* (Plenum, New York, 1978).
- [53] J. C. Slater, *The Self Consistent Field for Molecules and Solids: Quantum Theory of Molecules and Solids* (McGraw-Hill, New York, 1974), Vol. 4.
- [54] A. D. Becke, Phys. Rev. A, **38**, 3098 (1988)
- [55] J. P. Perdew, Phys. Rev. B, **33**, 8822 (1986).
- [56] J. Peeling, F. E. Hruska, and N. S. McIntyre, Can. J. Chem. **56**, 1555 (1978).
- [57] M. Stener, A. Lisini, and P. Decleva J. Electron. Spectr. Rel. Phenom. **69**, 197 (1994).

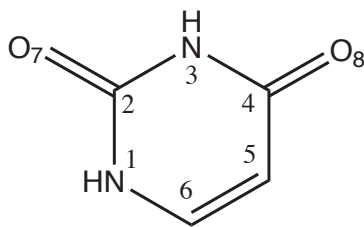


FIG. 1: Chemical structure for Uracil and numbering scheme adopted in the present work.

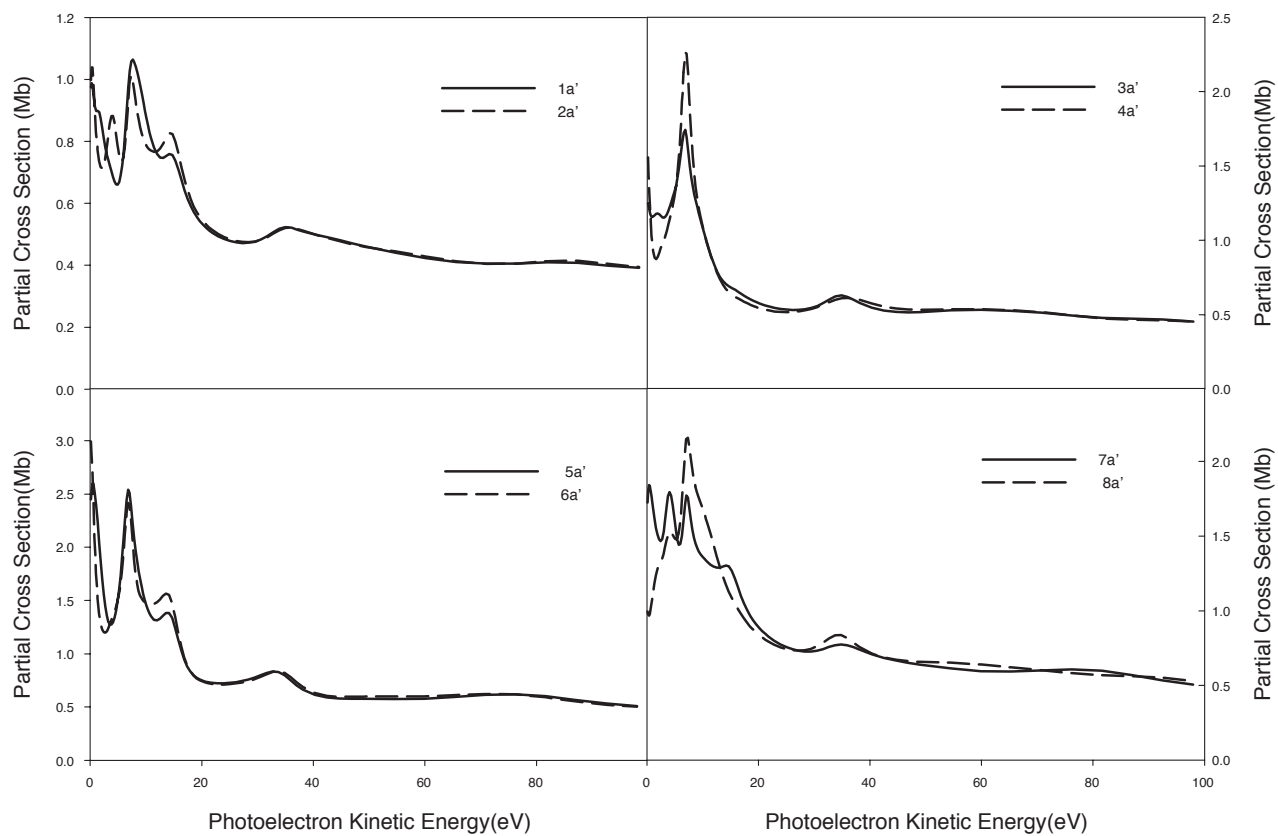


FIG. 2: LCAO DFT partial cross sections for 1s ionization of Oxygen (upper-left panel), Nitrogen (upper-right panel) and Carbon (lower panels) in the Uracil molecule.

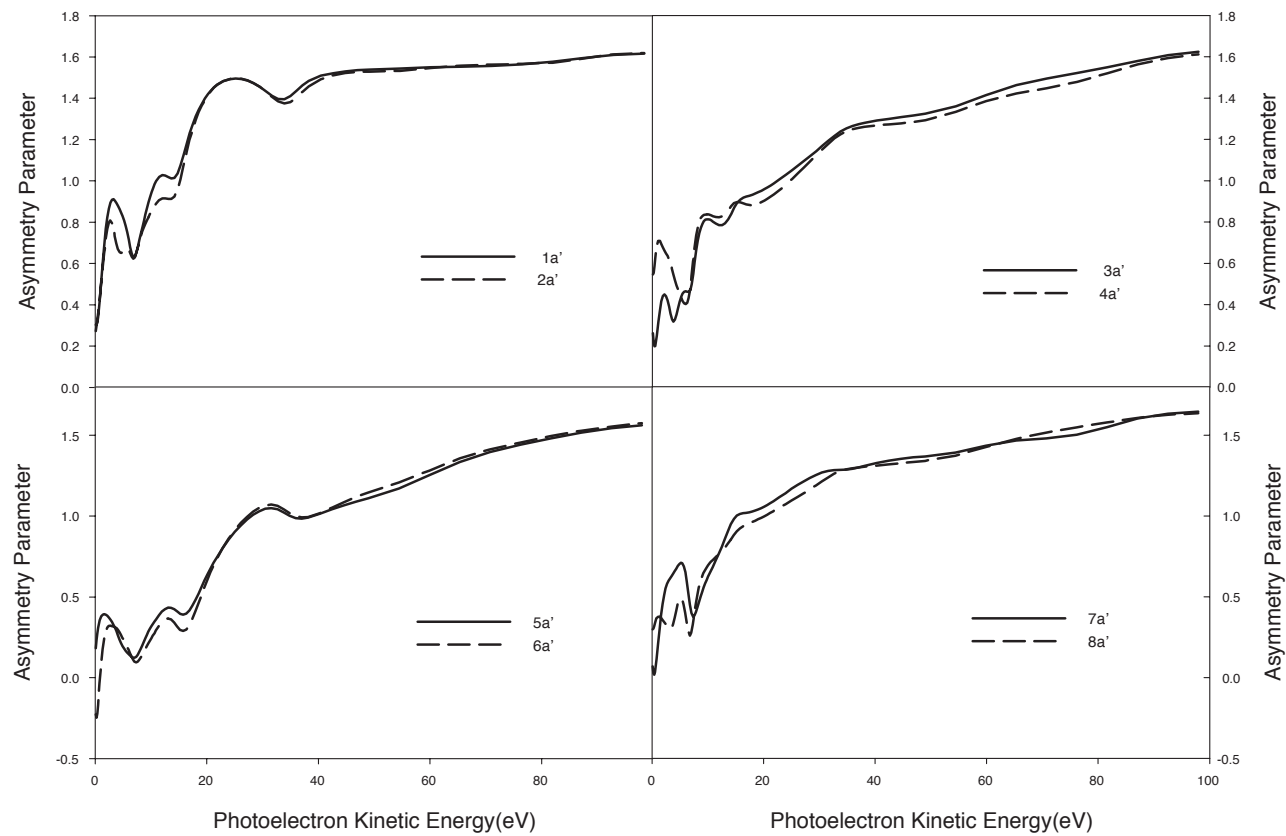


FIG. 3: LCAO DFT asymmetry parameter profiles for 1s ionization of Oxygen (upper-left panel), Nitrogen (upper-right panel) and Carbon (lower panels) in the Uracil molecule.

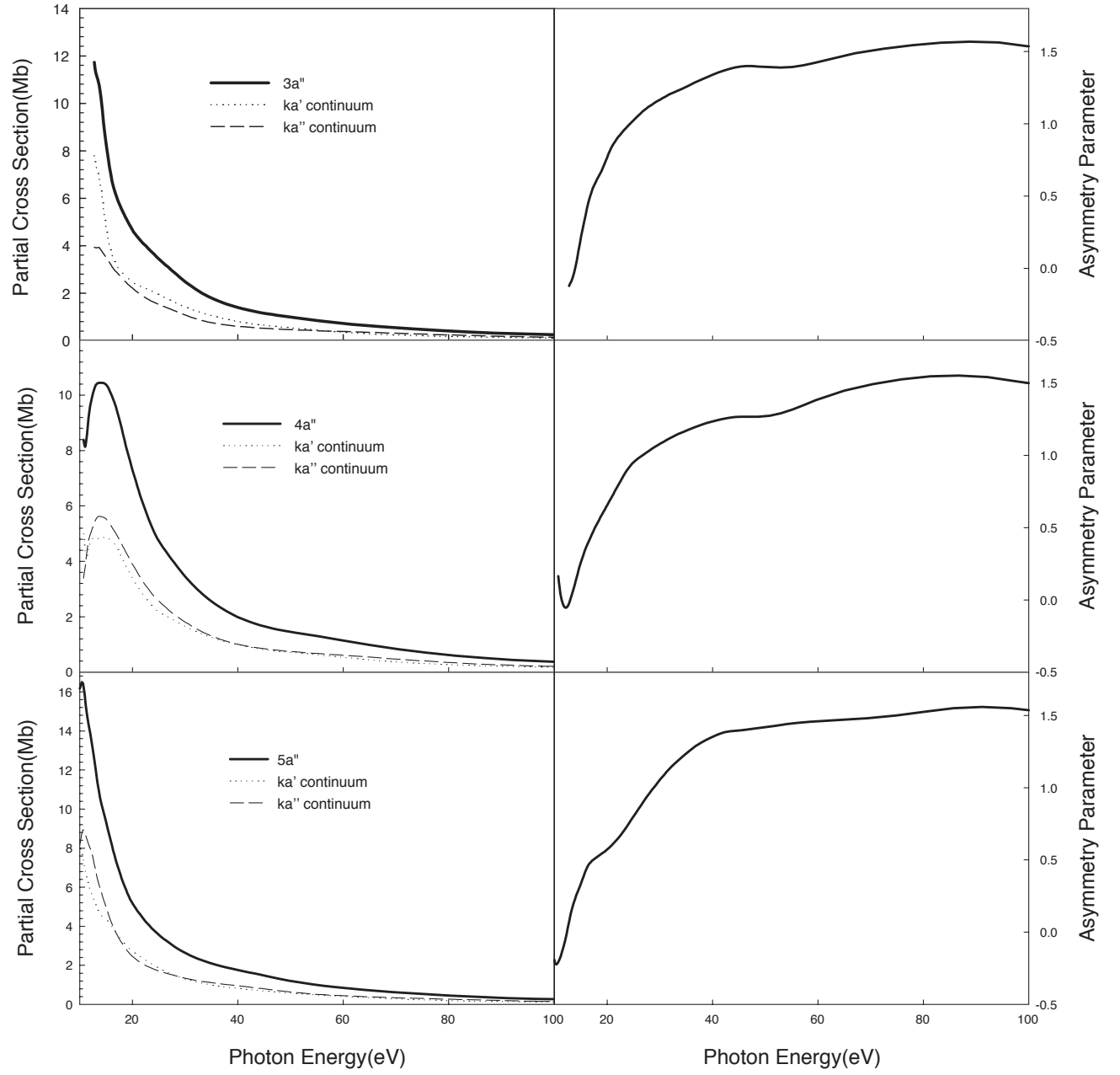


FIG. 4: LCAO DFT partial cross section and asymmetry parameter profiles for the $3a''$ (upper panels), $4a''$ (central panels), and $5a''$ (lower panels) orbital ionizations of Uracil.

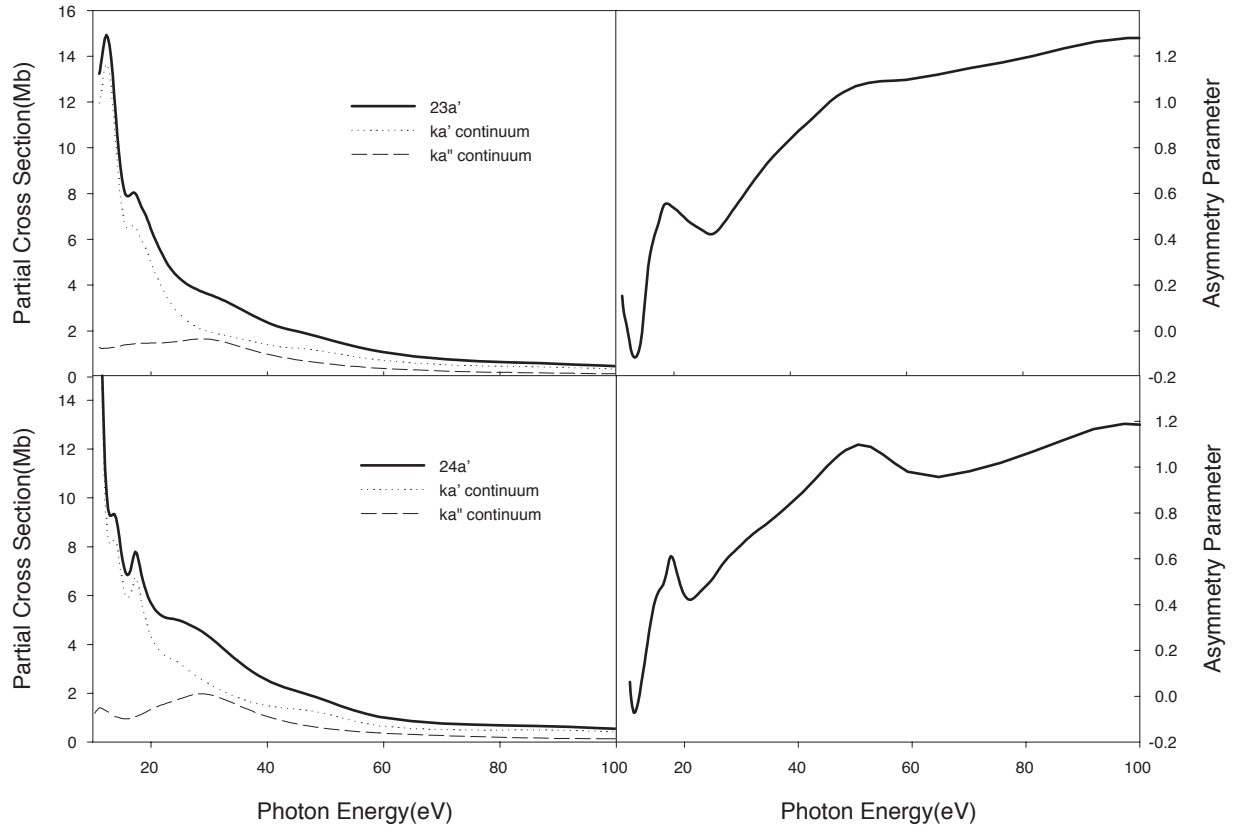


FIG. 5: LCAO DFT partial cross section and asymmetry parameter profiles for the $23a'$ (upper panels), and $24a'$ (lower panels) orbital ionizations of Uracil.

TABLE I: Uracil Ionization Energies (eV) (for the numbering scheme adopted, see Fig 1).

Orbital Ionization	P3 results ^a	DFT results, present work ^b	Exp. ^d
$1a'$ (O_71s)		536.8	531.8
$2a'$ (O_81s)		536.7	531.8
$3a'$ (N_11s)		406.9	400.8
$4a'$ (N_31s)		406.5	400.8
$5a'$ (C_21s)		294.3	289.7
$6a'$ (C_41s)		293.5	288.9
$7a'$ (C_61s)		292.6	286.8
$8a'$ (C_51s)		291.1	285.6
$3a''$ (π_3)	12.91	12.62 ^c	12.5-12.7
$23a'$ (n_2)	11.12	11.40 ^c	10.9-11.2
$4a''$ (π_2)	10.52	10.72 ^c	10.5-10.6
$24a'$ (n_1)	10.15	9.89 ^c	10.02-10.23
$5a''$ (π_1)	9.54	9.63 ^c	9.45-9.60

^aRef. 27, obtained with a 6-311G** basis set.

^bg.s. LB94 *xc* potential results, see text for details.

^ct.s. BP *xc* potential results, see text for details.

^dRefs. 24-26 and references therein.

TABLE II: Peak energy positions (photoelectron kinetic energy, eV) and symmetry of computed resonant states in the core and valence photoionization from Uracil.

Orbital Ionization	Peak position	Continuum symmetry
$1a'$	7.6, 14.1, 34.8	$\epsilon a'$
$2a'$	4.1, 7.3, 14.1, 35.9	$\epsilon a'$
$3a'$	6.8, 34.8	$\epsilon a'$
$4a'$	6.8, 35.9	$\epsilon a'$
$5a'$	0.5, 6.8, 14.1, 33.7	$\epsilon a'$
$6a'$	6.8, 14.1, 33.7	$\epsilon a'$
$7a'$	0.4, 4.1, 7.1, 14.1, 34.8	$\epsilon a'$
$8a'$	4.1, 7.3, 34.8	$\epsilon a'$
$23a'$	1.4, 6.0, 17.4	$\epsilon a', \epsilon a', \epsilon a''$
$4a''$	4.1, 3.3	$\epsilon a', \epsilon a''$
$24a'$	3.5, 7.1, 18.5	$\epsilon a', \epsilon a', \epsilon a''$
$5a''$	1.1	$\epsilon a''$